RSC Advances

PAPER

View Article Online
View Journal | View Issue

Cite this: *RSC Adv.*, 2019, **9**, 34837

AS1411 aptamer-modified theranostic liposomes co-encapsulating manganese oxide nano-contrast agent and paclitaxel for MRI and therapy of cancer†

Jingjing Li,[ab] Qing Li,[b] Meijuan He,[b] Fan Ding,[b] Lulu Cai,[b] Mingming Zhao,[b] Lina Dong,[b] Qi Wang[b] and Kai Xu*[ab]

Received 30th August 2019
Accepted 14th October 2019

DOI: 10.1039/c9ra06878c

rsc.li/rsc-advances

With the advantages and development of MRI nano-contrast agents (CAs), increasing number of MRI-based theranostic nanoparticles have emerged. Liposome, as a biosafe nanocarrier has been used phase III trial for cancer treatment. In this study, liposome was employed as a nanocarrier to co-encapsulate MRI nano-contrast agent poly(ethylene glycol)-grafted manganese oxide (PEG-MnO) and anticancer drug paclitaxel (PTX) for the fabrication of a novel theranostic nanocomplex. After being further modified with AS1411 aptamer, the obtained nanoprobe AS1411-liposome-PEG-MnO-PTX displayed the potential of simultaneous MRI diagnosis and therapy of renal carcinoma *in vitro* and *in vivo*. It was found that compared with PEG-MnO nano-CA, liposome-PEG-MnO and AS1411-liposome-PEG-MnO presented a stronger MR contrast enhancement effect in the tumor and longer retention time in the tumor region. More importantly, the introduction of AS1411 aptamer further enhanced the MRI effect and the tumor growth inhibition effect, showing its potential use as a theranostic nanoprobe for renal carcinoma.

Introduction

Theranostic nanocomplexes often take advantage of the high capacity of nanocarriers to ferry cargo that endows them with both imaging and therapeutic functions.[1] The family of nanocarriers includes polymer conjugates, polymeric nanoparticles, lipid-based carriers such as liposomes and micells, dendrimers, carbon nanotubes, gold nanoparticles, graphene oxide nanosheets, MoS_2 nanosheets, and SiO_2 nanoparticles.[2] Liposomes are vesicles consisting of amphiphilic phospholipids, such as phosphatidylcholine, phosphatidyl-ethanolamine, phosphatidylserine and phosphatidylglycerol to form a lipid bilayer with an aqueous core. They can encapsulate both hydrophobic and hydrophilic molecules. Liposomes have been well studied, mostly as drug delivery systems. Many liposome-based formulations have been actually in phase III trial for cancer treatment, such as ThermoDox for the release of doxorubucin in breast cancer[3] and lipoplatin for the controlled release of cisplatic in pancreatic, breast, non-small cell lung, head and neck cancers.[4–7] Except for the use as a drug delivery carrier, theranostic liposomes have been concerned more and more in recent years due to the demand of the simultaneous diagnosis and therapy. Such theranostic liposomes are commonly obtained by the co-encapsulation of drugs and imaging molecules, such as fluorescent quantum dots,[8,9] magnetic resonance imaging contrast agents (MRI CAs),[10–13] CT imaging contrast agents,[14] photoacoustic imaging CAs,[15] and ultrasound imaging CAs.[16] Among them, MRI-based theranostic liposomes own special advantages, because MRI is a widely used non-invasive medical imaging technique in clinical diagnosis. The commonly used MRI CAs are T_1-weighted CAs such as Gd-chelates[12,17] and T_2-weighted CAs such as magnetic nanoparticles.[18] Such encapsulation of MRI CAs in liposomes can not only realize the theranostics, but also improve the related properties of MRI CAs. For example, Gd-DTPA has been widely used as T_1 MRI contrast agent in the clinic. However, if not properly engineered, these small molecules generally present many limitations, such as very short blood circulation time and non-specific biodistribution, which may cause unwanted side effects.[19] Sessler *et al.* reported a MRI/fluorescence dual detection theranostic agent for liver cancer imaging in both subcutaneous and metastatic liver cancer murine models. A gadolinium texaphyrin core was first connected with a fluorescent prodrug doxorubicin *via* a disulfide bond. The quenched fluorescence of Dox by the paramagnetic Gd^{3+}-texaphyrine core could be recovered upon cleavage of the disulfide bond by cellular thiols. Then the conjugates were loaded into folate receptor-targeted liposomes for better solubility and prolonged blood circulation time as well as improved cancerous tissue targeting.[20] Zhao *et al.* developed MRI-guided liposomes with the co-encapsulation of MRI CA gadodiamide, hydrophilic drug carboplatin and hydrophobic drug paclitaxel for the simultaneous

[a]*Department of Radiology, Affiliated Hospital of Xuzhou Medical University, Xuzhou 221006, China. E-mail: qingchao0124@163.com; xkpaper@163.com*

[b]*School of Medical Imaging, Xuzhou Medical University, Xuzhou 221004, China*

† Electronic supplementary information (ESI) available: Fig. S1–S5. See DOI: 10.1039/c9ra06878c

therapy and diagnosis of lung tumors. The designed liposomes exhibited favorable biodistributions to tumors, and offered new possibilities for the simultaneous delivery of more than one drug and the evaluation of therapeutic response *in vivo* by T_1-enhanced MRI.[21] Dai *et al.* proposed a nanoscale magnetic nimodipine (NMD) delivery system for Parkinson's disease (PD) with liposome as nanocarrier and Fe_3O_4 as T_2 MRI CA. Compared with the free NMD group, they found that the Fe_3O_4-NMD-lips group presented a better neuroprotective effect and a 2.5-fold higher NMD concentration in the brain. Factional anisotropy values measured by MRI were employed to evaluate such therapy efficiency.[22] With the development of MRI CAs, nano-CAs including gadolinium oxide nanoparticles (Gd_2O_3 NPs) and manganese oxide nanoparticles (MnO NPs) emerged with improved contrast enhancement ability, longer blood circulation time and easy functionalization with targeting molecules. Their uses for tumor MRI *in vitro* and *in vivo* have been well documented and a few works have been reported on their combination with drugs for the fabrication of theranostic agents.[23–27] For example, Yan *et al.* developed ultrathin gadolinium oxide nanoscrolls to load an anticancer drug, DOX, which could be degraded in the tumor microenvironment for biocompatible MRI and biodegradation-enhanced cancer therapy.[28] Cypate-grafted gadolinium oxide nanocrystals (Cy-GdNCs) with cancer targeting capacity for trimodal NIRF/PA/MR imaging and pH-responsive photothermal therapy (PTT) were prepared by conjugating cypate with an albumin scaffold of GdNCs through a carbodiimide-catalyzed amide formation.[29] Chlorin e6 (Ce6)-grafted Gd_2O_3@albumin nanoplatform was proposed similarly for cancer imaging and photo-induced therapy.[30] Gadolinium oxide–gold nanocluster hybrid (Gd_2O_3–AuNCs) as a carrier for the delivery of indocyanine green (ICG) was applied as a theranostic agent for image-guided cancer therapy.[31] The excellent MRI behaviors of nano-CAs stimulated us to explore their applications in theranostics. Herein, we chose liposome as the nanocarrier to fabricate a theranostic liposome by co-encapsulating PEG-MnO NPs as the MRI CA and paclitaxel (PTX) as the drug for the simultaneous MRI diagnosis and therapy of renal carcinoma *in vitro* and *in vivo*. Manganese is considered as a safer metal than Gd, because it is not only an endogenous metal, but also an essential mineral in all biological systems.[32] The T_1 MRI relaxivity of our previously prepared PEG-MnO NPs was three times that of the clinically used contrast agent Magnevist (Gd-DTPA).[27] PTX is a microtubule inhibitor approved for the treatment of various cancer types, including breast, ovarian, non-small cell lung cancer, and head and neck carcinomas.[33] It works by promoting tubulin polymerization and microtubule stabilization, resulting in the arrest of mitosis at the G_2-M phase and mitotic cell death.[34,35] However, the poor aqueous solubility of PTX (less than 1 μg mL^{-1}) limits its use in the natural form. A hydrophobic lipid bilayer favors the loading of PTX. The fabricated theranostic nanoprobe, AS1411-liposome-PEG-MnO-PTX, displayed enhanced MRI of renal carcinoma and tumor growth inhibition in renal carcinoma tumor-bearing mice.

Experimental

Materials

1,2-Distearoyl-*sn*-glycero-3-phosphocholine (DSPC), cholesterol, 1,2-distearoyl-*sn*-glycero-3-phosphoethanolamine-*N*-[methoxy(polyethylene glycol)-2000] (DSPE-mPEG2000) and DSPE-mPEG2000-COOH were purchased from Xi'an Ruixi Biological Technology Co., Ltd (Xi'an, China). 1-Ethyl-3-(3-dimethylaminopropyl) carbodiimide hydrochloride (EDC·HCl), poly(ethylene glycol) bis-(carboxymethyl) ether 600 and *N*-hydroxysuccinimide (NHS) were obtained from Sigma-Aldrich. Methanol, chloroform, PTX, isopropanol and ethyl alcohol were obtained from Shanghai Aladdin Biochemical Technology Co., Ltd (Shanghai, China). AS1411 aptamer was ordered from Sinopharm Chemical Reagent Co., Ltd (Shanghai, China) as the following sequence: NH_2-AS1411: 5′-NH_2-C6-GGTGGTGGTGGTTGTGGTGGTGGTGG-3′.

Apparatus and characterization

The size and morphology characterization of blank liposomes and liposome-PEG-MnO nanocomplex were performed with a transmission electron microscope (TEM) (FEI Tecai G2F20, USA). The liposomes were stained using 3% tungstophosphoric acid for better visualization of the surface profile. The determination of Mn concentration in PEG-MnO and liposome-PEG-MnO nanocomplex was carried out with inductively coupled plasma-mass spectrometry (ICP-MS) (Optima 5300DV, PerkinElmer, USA). UV-vis absorption spectral analyses of liposome-PEG-MnO and AS1411-liposome-PEG-MnO as well as the PTX concentration determination were performed with HITACHI UH4150 Spectrophotometer (HITACHI, Japan). The absorbance values of MTT assay were determined by a microplate reader (Multiskon MK3, USA) at 490 nm. MRI scannings were performed on 3.0 T human magnetic resonance scanner (GE Signa, USA).

Cell culture and animal model development

The 786-0 renal carcinoma cells and normal human umbilical vein endothelial cell EA.hy926 were purchased from the Cell Bank of the Chinese Academy of Sciences (Shanghai, China). They were cultured in a humidified incubator (Thermo, USA) at 37 °C under 5% CO_2 atmosphere with 10% FBS-containing RPMI 1640 medium for 786-0 cells and 10% FBS-containing DMEM medium (Gibco, Grand Island, NY) for EA.hy926 cells, which were all supplemented with penicillin (100 μg mL^{-1}) and streptomycin (100 μg mL^{-1}).

Animal experiments were performed in accordance with the National Institutes of Health guidelines on the use of animals in research, and all animal experiments were approved by the Animal Care Committee of the Xuzhou Medical University. To develop a colon cancer-bearing mouse model, BALB/c mice maintained in a specific pathogen-free (SPF) environment were injected subcutaneously with a mixture of 100 μL of phosphate-buffered saline containing 5×10^6 786-O cells and 100 μL of Matrigel. Tumor-bearing mice were selected for the following *in vivo* experiments until the tumor was approximately 1.0 ×

1.0 cm ($L \times W$) (L is the ling diameter and W is the short diameter of a tumor).

Preparation of PEG-MnO nanoparticles with a polyol-like approach

PEG-MnO NPs were prepared *via* a polyol-like method according to our previous report.[27] In short, 1.004 g Mn $(NO_3)_2 \cdot 4H_2O$ was dissolved in 10 mL 1.985 mol L^{-1} poly(-ethylene glycol) bis-(carboxymethyl) ether 600. The solution was heated to 90–100 °C and then to 140 °C for 1 hour and to 180 °C for 4 hours. After being cooled to room temperature, the solution was dialyzed against ultrapure water (1 : 1000, v/v) to remove free Mn^{2+} and excess PEG. The membrane pore size was 3000 MW.

Preparation of blank liposome, PEG-MnO-encapsulated liposome (liposome-PEG-MnO) and AS1411 aptamer-modified liposome-PEG-MnO (AS1411-liposome-PEG-MnO)

Blank liposomes were prepared by lipid film hydration and extrusion method, with 1,2-distearoyl-*sn*-glycero-3-phosphocholine(DSPC), cholesterol, 1,2-distearoyl-*sn*-glycero-3-phosphoethanolamine-*N*-[methoxy(polyethylene glycol)-2000] (DSPE-mPEG2000) and DSPE-mPEG2000-COOH at a molar ratio of 1.10 : 1 : 0.15 : 0.15 according to the literature with minor modification.[36] Briefly, 0.0198 g DSPC, 0.0048 g cholesterol, 0.001875 g DSPE-mPEG2000 and 0.001875 g DSPE-mPEG2000-COOH were dissolved in a mixture of methanol (1 mL) and chloroform (4 mL). The above solution was ultrasonicated for 30 min with an ultrasonic cell disruptor. Then the organic solvents were evaporated, and a lipid film was formed after drying with nitrogen overnight. The obtained thin film was hydrated by vortexing in a 2 mL PBS solution and stirred to form blank liposomes. Finally, the blank liposomes were filtered through a 0.22 μm millipore membrane to get well size-distributed blank liposomes for further use.

For the preparation of liposome-PEG-MnO nanocomplex, the experimental steps were similar to that for blank liposomes but with minor modification. The obtained thin film was hydrated by vortexing in a 2 mL PEG-MnO solution and stirred to form liposome-PEG-MnO nanocomplex. After filtering through a 0.22 μm millipore membrane, the obtained liposome-PEG-MnO nanocomplex was further ultrafiltrated to remove the unencapsulated PEG-MnO nanoparticles (MW = 30 kDa).

For AS1411 aptamer modification, 1 mg EDC was dissolved in liposome-PEG-MnO nanocomplex solution (2 mL) and incubated at 37 °C for 15 min. Then, 1 mg NHS and 20 μL 250 μM AS1411 aptamer were added and reacted at 37 °C for 2 h. Finally, the mixture was centrifuged, washed with water and the precipitate was dispersed in 2 mL PBS for further use.

MR T_1 relaxivity calculation of PEG-MnO nanoparticles and liposome-PEG-MnO nanocomplex

Relaxivity values of PEG-MnO NPs and liposome-PEG-MnO nanocomplex were determined by measuring the longitudinal proton relaxation time (T_1) as a function of Mn concentration. The T_1 relaxation times of various concentrations of PEG-MnO NPs and liposome-PEG-MnO nanocomplex were obtained by MRI scanning. The following parameters were adopted in data acquisition as described in our previous report:[37] ① T_1-weighted images: echo time (TE) = 16.5 ms, repetition time (TR) = 425 ms, field of view (FOV) = 14 cm × 14 cm, matrix = 384 × 256, slice thickness = 2.0 mm, spacing = 1.5 mm; ② T_1-map images: TE = 7.4 ms, TR = 200–800 ms, FOV = 14 cm × 14 cm, matrix = 384 × 256, slice thickness = 2.0 mm, spacing = 1.5 mm. Quantitative T_1 relaxation maps were reconstructed from datasets using function software at a workstation (ADW 4.2).

Loading of PTX drug with liposome-PEG-MnO nanoparticles

To load PTX as much as possible, different PTX amounts were introduced to look for the optimized concentration for the preparation of liposome-PEG-MnO-PTX nanocomplex. Briefly, 0.0198 g DSPC, 0.0048 g cholesterol, 0.001875 g DSPE-mPEG2000, 0.001875 g DSPE-mPEG2000-COOH and PTX (2 mg, 3 mg, 4 mg and 5 mg) were dissolved in a mixture of methanol (1 mL) and chloroform (4 mL). The other experimental details were the same as that for liposome-PEG-MnO nanocomplex described above.

Prior to calculating the encapsulation and drug loading efficiency, the linear regression equation for PTX UV-vis absorption *versus* concentration was first constructed. To begin with, 100 μg mL^{-1}, 80 μg mL^{-1}, 60 μg mL^{-1}, 40 μg mL^{-1}, and 20 μg mL^{-1} PTX solutions were prepared by simply dissolving PTX in a demulsifier, which consisted of isopropanol, absolute ethyl alcohol, and ether at a ratio of 2 : 2 : 1 (v/v). Then, their UV-vis absorptions at 230 nm were recorded. For the determination of encapsulation efficiency, liposome-PEG-MnO-PTX nanocomplexes with different amounts of PTX (2 mg, 3 mg, 4 mg and 5 mg) were centrifuged at 15 000 rpm for 15 min, and the PTX concentrations in liposome-PEG-MnO-PTX nanocomplexes were determined from the UV-vis spectra after demulsification. For the determination of the loading efficiency, the obtained amount of liposome-PEG-MnO-PTX was weighted after vacuum freeze-drying. The calculation methods are listed below.

$$\text{Encapsulation efficiency (\%)} = m_{\text{PTX}}/m_{\text{PTX, total}} \times 100$$

$$\text{Loading efficiency (\%)} = m_{\text{PTX}}/m_{\text{liposome-PEG-MnO-PTX}} \times 100$$

Evaluation of the *in vitro* release of PTX from liposome-PEG-MnO PTX and liposome-PTX

The release of PTX from liposome was observed using the dialysis method at 37 °C according to the literature with some slight modification.[38,39] Briefly, 1 mL liposome-PEG-MnO-PTX or liposome-PTX was placed in a dialysis bag (MWCO 10 kDa) and dialyzed against 30 mL release medium (PBS and SDS, pH = 7.4) with magnetic stirring. At the scheduled time points (0.5 h, 1 h, 2 h, 3 h, 4 h, 5 h, 8 h, 10 h, 12 h, 18 h, 24 h, 36 h, 48 h and 72

h), the concentrations of the released PTX were measured using the UV-vis absorption spectra.

MTT assay to evaluate the cell biocompatibility of liposome-PEG-MnO nanocomplex and the drug-mediated cytotoxicity of liposome-PTX, AS1411-liposome-PEG-MnO, liposome-PEG-MnO-PTX and AS1411-liposome-PEG-MnO-PTX nanocomplex

786-0 cells were plated in 96 well plates at a concentration of 5×10^5 cells per mL per well and incubated for 24 h at 5% CO_2, 37 °C. Then, different concentrations of liposome-PEG-MnO nanocomplex or AS1411-liposome-PEG-MnO (0, 0.05, 0.1, 0.15, 0.2, 0.25, 0.3, 0.35, 0.4 mM Mn) were added and the cells were cultured for another 24 h. After discarding the liposome-PEG-MnO nanocomplex and washing twice with PBS buffer, RPMI 1640 containing MTT (5 mg mL^{-1}) was added and further incubated for 4 h at 5% CO_2, 37 °C. Finally, the media containing MTT were removed and the formazan crystal precipitates were solubilized in 100 μL of dimethyl sulfoxide (DMSO). After shaking for 15 min at 37 °C, the absorbance at 490 nm was measured on BioTek Epoch microplate reader (Multiskon MK3, USA). The cell viability was determined relative to the untreated control cells. The toxicity of liposome-PEG-MnO nanocomplex on EA.hy926 cells was tested with the same procedure.

The evaluation of the drug-mediated cytotoxicity of liposome-PTX, AS1411-liposome-PEG-MnO, liposome-PEG-MnO-PTX nanocomplex and AS1411-liposome-PEG-MnO-PTX nanoprobe on 786-0 cells were performed similarly. The treated concentrations were 24 mg L^{-1} PTX.

In vivo toxicity evaluation of liposome-PEG-MnO and AS1411-liposome-PEG-MnO

The *in vivo* toxicity of liposome-PEG-MnO nanocomplex was evaluated by monitoring the weight changes of mice and histological changes of several organs (heart, liver, spleen, kidney and lung) post-injection of liposome-PEG-MnO nanocomplex. Six BALB/c mice with similar weight were randomly divided into two groups, experimental group and control group. In the experimental group, 300 μL liposome-PEG-MnO nanocomplex (4 mM Mn) was injected into the tail vein of BALB/c mice. In the control group, no treatment was performed on the mice. At 0, 1, 2, 3, 4, 5, 7, 11, 14, 21 and 30 day, the six mice were weighted, respectively. For the histological study, the mice were dissected post-injection of liposome-PEG-MnO nanocomplex or AS1411-liposome-PEG-MnO after 24 hours or 1 week. The obtained organs were fixed in 10% formalin, respectively. After being dehydrated with xylene and graduated alcohol, the tissues were stained with hematoxylin and eosin (H&E). The mice without treatment were also dissected as controls.

Determination of blood circulation half-life of liposome-PEG-MnO nanocomplex

The method of determination of the blood circulation half-life of liposome-PEG-MnO nanocomplex was the same as in our previous report.[39] First, 300 μL liposome-PEG-MnO nanocomplex (4 mM Mn) was injected *via* tail-vein into the BALB/c mice. Then, 10 μL peripheral blood was collected from the tail vein at different time points (5, 15, 30, 45, 60, 120, 180, 240, 360, 720 and 1440 minutes). The obtained blood was mixed with heparin sodium (90 μL) in separate tubes and digested with HNO_3 for Mn concentration determination by ICP-MS.

In vivo MRI of renal carcinoma tumor-bearing mice with PEG-MnO, liposome-PEG-MnO and AS1411-liposome-PEG-MnO

To compare the MRI behaviors of PEG-MnO NPs, liposome-PEG-MnO nanocomplex and AS1411-liposome-PEG-MnO nanoprobes on renal carcinoma tumor *in vivo*, twelve tumor-bearing mice were divided into three groups randomly: PEG-MnO group, liposome-PEG-MnO group and AS1411-liposome-PEG-MnO group. The mice in each group were anesthetized by the intraperitoneal injection of 2% mebumalnatrium (4 μL g^{-1} body weight), and it was followed by tail-vein administration of PEG-MnO NPs, liposome-PEG-MnO nanocomplex and AS1411-liposome-PEG-MnO nanoprobes (300 μL nanomaterials with the Mn concentration of 4 mM), respectively. Then, T_1WI images were acquired and the signal intensities of the tumors were determined at scheduled intervals on 3.0 T MR imaging system (GE Discovery 750W, USA) with the animal T/R coil (Magtron Inc., Jiangyin, China). The sequences for the T_1-weighted images were set as follows: TE = 12 ms; TR = 400 ms; FOV = 80 mm × 80 mm; slice thickness = 2 mm; slicing = 0.2 mm; and matrix = 256 × 256. To compare the signal intensity at different time points, the same protocols, prone position and the same scanning landmark of MRI were required. The relative intensity changes of the same region of interest on the same slice in the same window width and window level were recorded by software at the workstation GE AW4.6.

Determination of *in vivo* anticancer efficiency of blank liposome, liposome-PTX, liposome-PEG-MnO-PTX, and AS1411-liposome-PEG-MnO-PTX

Tumor-bearing mice were randomly divided into 5 groups (n = 5), which were post-injection of saline for Group 1, blank liposome for Group 2, liposome-PTX for Group 3, liposome-PEG-MnO-PTX for Group 4, and AS1411-liposome-PEG-MnO-PTX for Group 5 every 3 days. Except for Group 1 and Group 2, the PTX concentration of the other groups was set to be 7.5 mg kg^{-1}. During the course of treatment, the mice's tumor sizes were measured every 2 days and the MRI scannings were carried out every 7 days. The formula for the calculation of tumor volume is as follows:

$$V = (W^2 \times L)/2$$

Statistical analysis

Statistical analyses were carried out with SPSS 16.0 software (Chicago, IL). One-Way Anova and Dunnett's tests were used to compare the statistical significance between different groups. Data are presented as mean ± SD. $p < 0.05$ was considered significantly different.

Results and discussion

Synthesis and characterization of blank liposomes, liposome-PEG-MnO and liposome-PEG-MnO-PTX nanocomplex

The synthesis of theranostic liposome was usually realized by the encapsulation of drug and signal reporter during the formation of liposome. There are several methods reported for the preparation of liposomes. In 1965, Bangham method or thin lipid film hydration method was first reported.[40] It consists of the formation of a thin film of lipids after the evaporation of organic solvents followed by freeze-drying to ensure the complete elimination of solvents. Other approaches such as the reverse phase evaporation technique,[41] the solvent injection technique,[42] and the double emulsion technique have also been described. Herein, blank liposomes, liposome-PEG-MnO nanocomplex and liposome-PEG-MnO-PTX nanocomplex were prepared by the thin film hydration method, followed by membrane extrusion. PEG-MnO NPs were first prepared, and the related characterizations of PEG-MnO NPs can be found in our previous report.[27] TEM images in Fig. 1 show that the obtained blank liposomes and liposome-PEG-MnO nanocomplex were spherical with an average size of 120.89 nm and 133.87 nm, respectively. Compared with the blank liposomes, the black color in the core of liposome-PEG-MnO nanocomplex indicated the successful encapsulation of PEG-MnO NPs.

MRI behaviors of PEG-MnO NPs and liposome-PEG-MnO nanocomplex

As MRI contrast agents, PEG-MnO NPs have presented good MRI performance for tumor imaging. Whether they can preserve their property or have better behavior in liposome-PEG-MnO nanocomplex should be evaluated. To achieve this aim, the T_1 relaxation times of PEG-MnO NPs and liposome-PEG-MnO nanocomplex with the same Mn concentration were determined and compared. As shown in Fig. 2A, compared with water (2037.80 ± 4.71 ms), both PEG-MnO NPs (526.60 ± 3.90 ms) and liposome-PEG-MnO nanocomplex (272.33 ± 4.37 ms) presented shorter T_1 relaxation times with significant statistical differences ($p < 0.05$). Meanwhile, the T_1 relaxation time of liposome-PEG-MnO nanocomplex was significantly shorter than that of PEG-MnO NPs ($p < 0.05$), indicating a stronger MRI signal enhancement ability of liposome-PEG-MnO nanocomplex. Then, the MRI relaxivity values of PEG-MnO NPs and liposome-PEG-MnO nanocomplex were determined by measuring the longitudinal (T_1) proton relaxation time as a function of Mn concentration at 3.0 T. As expected, liposome-PEG-MnO nanocomplex displayed a higher r_1 value (14.45 *vs.* 7.61 s^{-1} mM^{-1} Mn, Fig. 2B and C), which might have come from the increased molecular size after encapsulation in liposomes.[37] As reported, in a certain range, the larger the size of nanoparticles, the stronger the saturation magnetization and relaxation rate of the nanomaterials is.[43] Theoretically, the proton relaxivity of the contrast agent is determined by the following equation:

$$r_1 = Cq\mu_{\text{eff}}{}^2\tau_c r^{-6}$$

where C is a constant, q is the number of inner sphere water molecules, μ_{eff} is the effective magnetic moment, τ_c is the molecular correlation time, and r is the metal ion···H (H_2O) distance.[44,45] The molecular correlation time τ_c is determined by the rotational correlation time τ_r, the electronic correlation time τ_s, and the proton residence time τ_m, as expressed in the equation ${\tau_c}^{-1} = {\tau_r}^{-1} + {\tau_s}^{-1} + {\tau_m}^{-1}$.[46] Changing the molecular

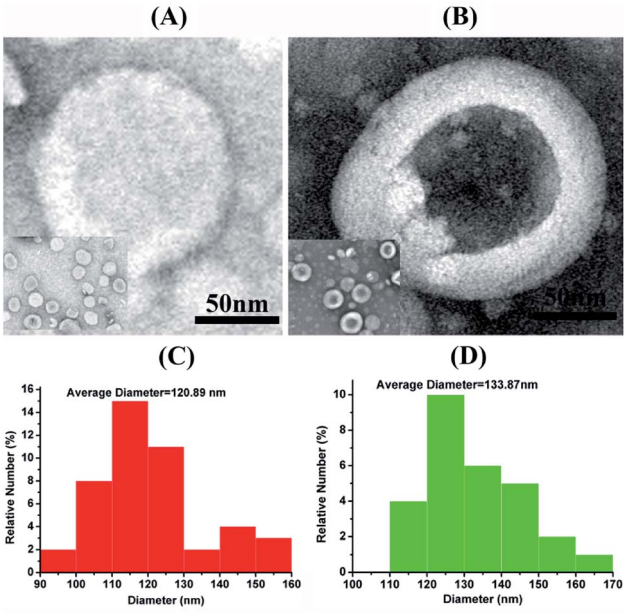

Fig. 1 TEM images of liposome (A) and liposome-PEG-MnO (B). Size distribution of liposome (C) and liposome-PEG-MnO (D).

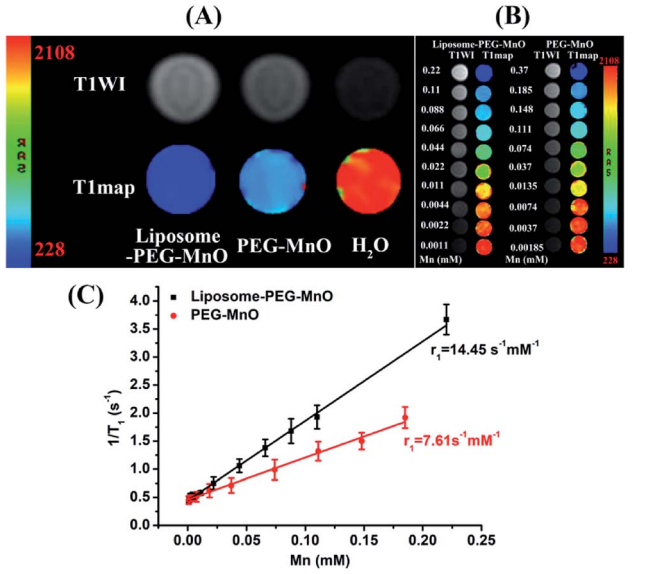

Fig. 2 (A) T_1-weighted MR images and T_1-map images of liposome-PEG-MnO, PEG-MnO and H_2O. (B) T_1-weighted MR images and T_1-map images of liposome-PEG-MnO and PEG-MnO with different concentrations. (C) T_1 relaxivity curves of PEG-MnO and liposome-PEG-MnO.

size is one of the possible approaches to increase τ_r.[47] Lanza also reported that the relaxivity of MnO nanoparticles could be tuned by the manipulation of their size and curvature.[48] Coating of nanoparticles can significantly improve their relaxivity. Gilad *et al.* found that mesoporous silica-coated hollow manganese oxide (HMnO@mSiO_2) nanoparticles presented a higher longitudinal relaxation enhancement of water protons.[49] These results indicated the promising potential of liposome-PEG-MnO nanocomplex as a T_1 MRI contrast agent.

In vitro and *in vivo* toxicity test of liposome-PEG-MnO nanocomplex

Prior to being used as a T_1 MRI CA, the biocompatibility of liposome-PEG-MnO nanocomplex should be evaluated first. Its *in vitro* cytotoxicities on 786-0 cells and EA.hy926 cells were evaluated with MTT assay. Different amounts of liposome-PEG-MnO nanocomplex were treated with 786-0 cells and EA.hy926 cells, respectively. As shown in Fig. 3A, no significant cytotoxicity was observed even with the concentration of 0.4 M Mn, no matter on 786-0 cells or EA.hy926 cells, indicating the excellent cell biocompatibility of liposome-PEG-MnO nanocomplex. Then, we intravenously injected liposome-PEG-MnO nanocomplex into mice to evaluate its *in vivo* toxicity. As shown in Fig. 3B, nearly all mice decreased in weight in the first two days, followed by a return of both groups to the initial weight and beyond. This meant that there was no detectable systemic toxicity of liposome-PEG-MnO nanocomplex. Also there was no acute toxicity observed during and after the experiment. Furthermore, the histological analysis showed that no obvious histopathological abnormalities were observed in the major organs (heart, liver, spleen, kidneys and lungs), indicating that no tissue damage occurred as a result of the injection of liposome-PEG-MnO nanocomplex (Fig. 3C). After modification with AS1411 aptamer, AS1411-liposome-PEG-MnO also displayed a similar cytocompatibility and no tissue damage *in vivo* (Fig. S1†). As we all know, AS1411 aptamer can be used for the inhibition of tumor cells. But in this work, AS1411-liposome-PEG-MnO exhibited no obvious cytotoxicity in 786-O cells within the examined concentration range. We ascribed such a result to the relatively low concentration of AS1411 aptamer. The concentrations of AS1411 aptamer in each group in Fig. S1† were determined to be 46 nM, 92 nM, 138 nM, 184 nM, 230 nM and 276 nM, respectively. As reported in the literature, the IC50 of AS1411 aptamer was at around 2 μM concentration range, and a 7 day exposure of AS1411 aptamer at 10 μM dose could induce more than 60% killing of three leukemia and two of three lymphoma cell lines.[50,51] Zhang's group also reported similar results that AS1411 aptamer within 0 to 400 nM displayed no obvious cytotoxicity on human ovarian cancer cell lines (SKOV3 and OVCAR3) and human normal liver cell line (L02).[52] Liposome-PEG-MnO nanocomplex displayed a longer blood circulation half-life of 333.35 min, which was 5.6 times that of PEG-MnO NPs (59.76 min),[27] favoring their effective accumulation in the tumor tissue to enhance MRI sensitivity (Fig. S2†). Such a long circulation time might come from the existence of liposome and PEG coating.[17,53–55]

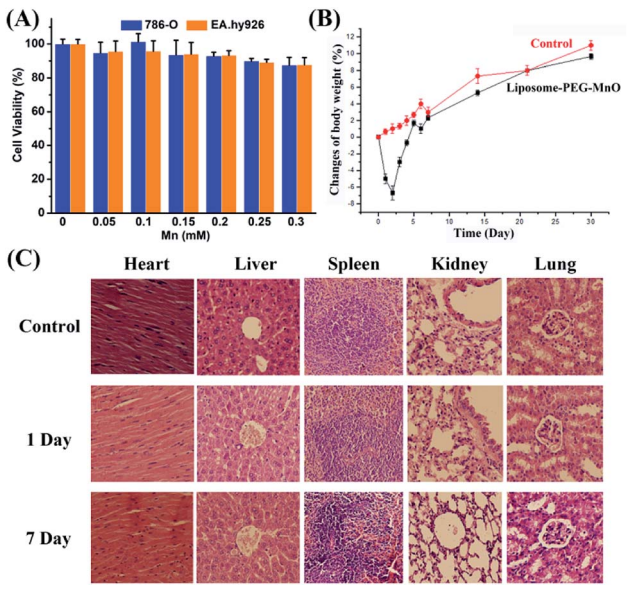

Fig. 3 . (A) Cell viability of 786-O cells and EA.hy926 cells incubated with different concentrations of liposome-PEG-MnO nanocomplex. (B) The changes in body weight of mice post-injection of saline or liposome-PEG-MnO nanocomplex. (C) Histological images of the heart, liver, spleen, kidney and lung of mice 1 day or 7 day post-injection of liposome-PEG-MnO nanocomplex.

In vivo MRI of renal carcinoma with PEG-MnO NPs, liposome-PEG-MnO nanocomplex, and AS1411-liposome-PEG-MnO nanoprobe

To systematically evaluate the MRI performances and biodistribution of PEG-MnO NPs, liposome-PEG-MnO nanocomplex, and AS1411-liposome-PEG-MnO nanoprobe *in vivo*, twelve tumor-bearing mice were randomly divided into three groups: PEG-MnO group, liposome-PEG-MnO group and AS1411-liposome-PEG-MnO group. AS1411 aptamer can recognize nucleolin and internalize in a variety of cancer cells, such as renal, breast and other adenocarcinoma cell lines. It has been widely used as a targeting molecule for specific tumor cell recognization and drug delivery system.[56–60] In this work, amino group-modified AS1411 aptamer was conjugated with carboxyl group-coating liposome-PEG-MnO nanocomplex by the covalent coupling reaction. The successful conjugation of AS1411 aptamer to liposome-PEG-MnO nanocomplex was confirmed by UV-vis spectra and zeta potential determinations (Fig. S3†). In each group, the mice were intravenously injected with the related nanomaterials with the same amount of Mn *via* the tail vein and a series of MRI images were collected at scheduled intervals post-injection. As shown in Fig. 4, in all groups, compared with pre-injection references, high contrast enhancements at tumor, liver, kidneys and heart were observed after injection. But in different groups, the signal enhancement degree, the enhancement last time and the metabolic pathway varied. In the PEG-MnO group, the contrast intensity in the tumor was increased with time and reached a maximum at 15 min post-injection. The signal in the tumor returned to the

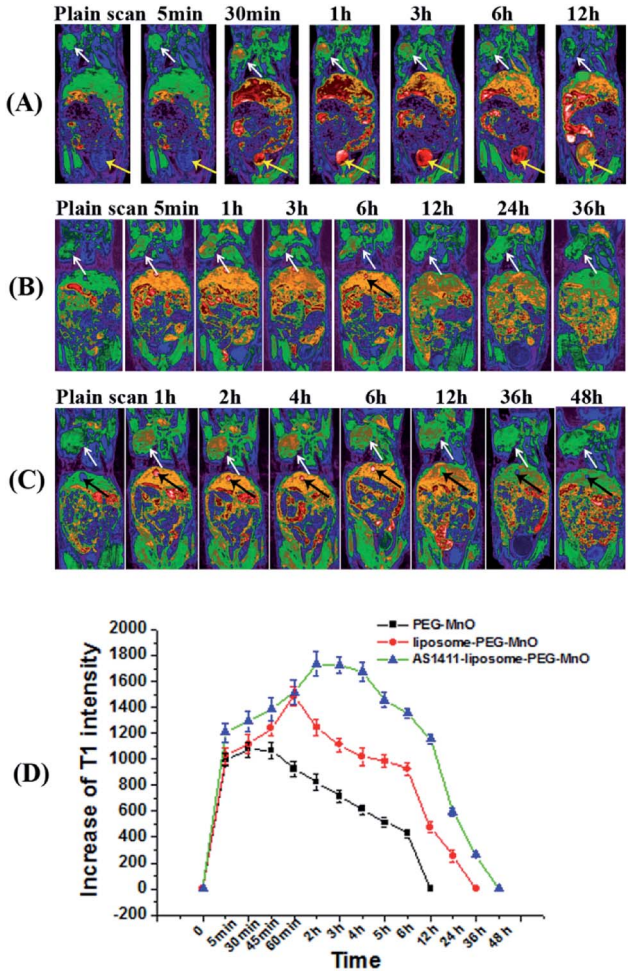

Fig. 4 Pseudo-color MR T_1 images of mice bearing renal carcinoma tumors pre- and post-injection of PEG-MnO NPs (A), liposome-PEG-MnO NPs (B) and AS1411-liposome-PEG-MnO nanoprobes (C). (D) The changes in signal intensity of tumor at different time points in the above three groups. The white, yellow and black arrows indicate tumor, bladder and gallbladder, respectively.

plain scanning after 12 hours. The high signal in the bladder indicated that the injected PEG-MnO NPs were cleared from the body through the urinary system. In the liposome-PEG-MnO group, the signal enhancement degree in the tumor was stronger than that in the PEG-MnO group, and the maximum signal occurred at 1 h post-injection of liposome-PEG-MnO nanocomplex. Such enhancement disappeared gradually within 36 h. Different from PEG-MnO NPs, the injected liposome-PEG-MnO nanocomplex could not be observed in the bladder. Instead, a signal enhancement in the gallbladder became obvious with the time passing by, indicating that the excretion of liposome-PEG-MnO nanocomplex was mainly *via* the hepatobiliary system. In the AS1411-liposome-PEG-MnO group, the maximum signal enhancement appeared at 2 h post-injection of AS1411-liposome-PEG-MnO nanoprobe. Such signal began to reduce after 4 h and disappeared after 48 h. Similarly with liposome-PEG-MnO nanocomplex, the injected AS1411-liposome-PEG-MnO nanoprobes were excreted from the body *via* the hepatobiliary system. The stronger signal enhancement and longer retention time in the AS1411-liposome-PEG-MnO group might come from the existance of AS1411 aptamer. The specific binding of AS1411 aptamer to nucleolin that is overexpressed on the surface of 786-0 cells and the internalization ability into cells increased the amount and retention time of AS1411-liposome-PEG-MnO nanoprobes in the tumor region. The different metabolic pathways of PEG-MnO NPs and liposome-PEG-MnO nanocomplex were ascribed to their different sizes. As reported, the clearance pathway of nanomaterials was closely related to their sizes. The nanoparticles with a hydrodynamic diameter below 5–6 nm could be cleared rapidly from the body by renal filtration and urinary excretion, while those with a hydrodynamic diameter above 10–20 nm were usually captured and eliminated through the liver, into bile and into feces.[61] These results showed that the encapsulation of PEG-MnO NPs into liposomes could not only enhance the contrast enhancement in the tumor, but also extend their retention time. More importantly, the presence of AS1411 aptamer further strengthens such effect, favoring their applications in tumor imaging.

Determination of the encapsulation and loading efficiencies of paclitaxel with liposome-PEG-MnO nanocomplex and the drug release *in vitro*

To further apply liposome-PEG-MnO nanocomplex as a theranostic agent, paclitaxel as a model drug was introduced to be encapsulated in it. As a drug carrier, liposome should load as much PTX as possible and be able to release it in a sustained manner. With the introduction of different amounts of PTX, the related encapsulation and loading efficiencies were determined from the absorption peak at 230 nm in the UV-vis spectrum of PTX (Fig. S4†). As shown in Fig. S5,† with different PTX amounts involved, different encapsulation and drug loading efficiencies were obtained. At the optimized condition, the encapsulation and drug loading efficiencies were 79.81% and 12.87%, respectively. Then, the *in vitro* PTX release property was evaluated *via* the direct dispersion method in PBS (pH 7.4) containing 0.1% (v/v) SDS at 37 °C. It was seen that the release of PTX was faster in the case of liposome-PEG-MnO-PTX than that of

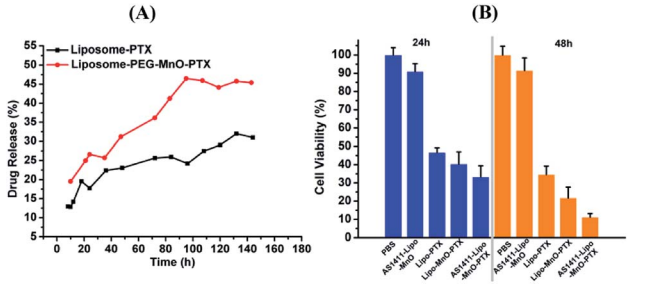

Fig. 5 (A) The release percentages of PTX from liposome-PTX and liposome-PEG-MnO-PTX in PBS solutions (pH = 7.4, 37 °C). (B) Cell viability of 786-O cells after incubation with PBS, AS1411-liposome-PEG-MnO, liposome-PTX, liposome-PEG-MnO-PTX and AS1411-liposome-PEG-MnO-PTX for 24 h and 48 h.

liposome-PTX (Fig. 5A). But compared with the release of PTX from Taxol®, the release of PTX encapsulated in the liposomes was much slower because lipid bilayers are stabilized by cholesterol and/or Tween 80, which favorsed the stability of the drug in the blood circulation.[38] With 24 mg L^{-1} PTX, the cytotoxicity of PBS, liposome-PTX, liposome-PEG-MnO-PTX and AS1411-liposome-PEG-MnO-PTX were evaluated after 24 h and 48 h incubation with 786-O cells. As shown in Fig. 5B, obvious cytotoxicities were observed in the presence of liposome-PTX, liposome-PEG-MnO-PTX and AS1411-liposome-PEG-MnO-PTX, and the latter two nanocomplexes displayed higher cell growth inhibition rates, which might come from the higher drug release rate and the targeting ability of AS1411 aptamer.

In vivo inhibition of tumor growth

Finally, the *in vivo* inhibition effects of the fabricated nanocomplex on tumor growth were further evaluated. The photographs of the tumor-bearing nude mice and tumorous autopsy in different treatment groups are shown in Fig. 6A It shows that the tumor size of the saline group looks similar to that of the blank liposome group, both of which are larger than the other three groups, liposome-PTX group, liposome-PEG-MnO-PTX group, and AS1411-liposome-PEG-MnO-PTX group. The changes in tumor size post-injection of the drug in each group are compared in Fig. 6B, and AS1411-liposome-PEG-MnO-PTX presents the best tumor growth inhibition effect. MRI scannings were performed during the whole course to monitor the tumor growth changes (Fig. 6C). The results indicated that our fabricated AS1411-liposome-PEG-MnO-PTX nanoprobe could enhance the antitumor growth effectively.

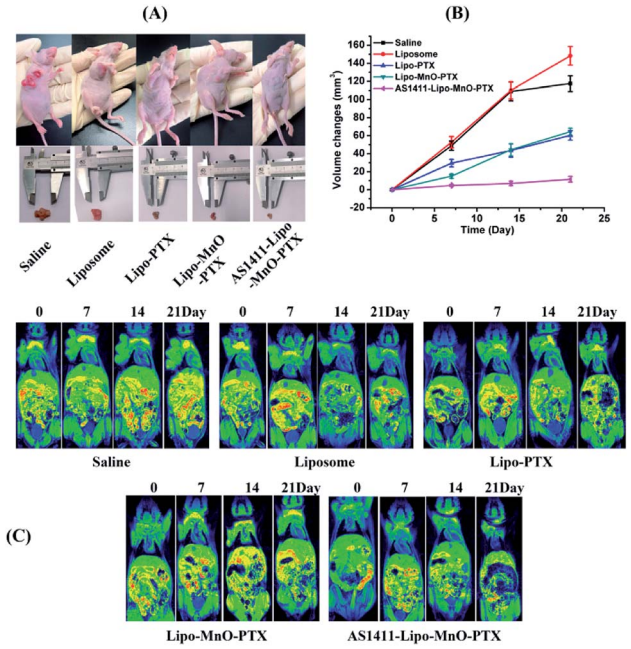

Fig. 6 (A) Representative images of the 786-O tumors of the mice after treatment with saline, liposome, liposome-PTX, liposome-PEG-MnO-PTX and AS1411-liposome-PEG-MnO-PTX. (B) *In vivo* antitumor therapeutic efficacy of saline, liposome, liposome-PTX, liposome-PEG-MnO-PTX and AS1411-liposome-PEG-MnO-PTX. (C) Representative pseudo-color MR T_1 images of mice bearing renal carcinoma tumors pre- and post-injection of saline, liposome, liposome-PTX, liposome-PEG-MnO-PTX and AS1411-liposome-PEG-MnO-PTX.

Conclusions

Herein, we fabricated a novel theranostic nanoprobe, AS1411-liposome-PEG-MnO-PTX for the simultaneous diagnosis and therapy of renal carcinoma. Compared with PEG-MnO nano-CA, the T_1 relaxivity of liposome-PEG-MnO was increased from 7.61 to 14.45 s^{-1} mM^{-1}. The *in vivo* MRI and the inhibition of tumor growth effect further testified the excellent behavior of our fabricated AS1411-PEG-MnO-PTX theranostic nanocomplex. The results indicated that the presence of liposome not only favored the co-existence of MRI nano-CA and the anticancer drug, but also improved the MRI ability of nano-CA, which is better for the low-dose use of CA or the clear imaging of lesions.

Conflicts of interest

There are no conflicts to declare.

Acknowledgements

This work was supported by the National Natural Science Foundation of China (81771904, 81874183), Natural Science Foundation of Jiangsu Province for the Excellent Young Scholars (BK20170054), China Postdoctoral Science Foundation (2016M601890, 177607), Qing Lan Project, the Peak of Six Talents of Jiangsu Province (WSN-112), Jiangsu Provincial Medical Youth Talent (QNRC2016776), and Six one project of Jiangsu Province (LGY2018083).

Notes and references

1 J. Xie, S. Lee and X. Chen, *Adv. Drug Delivery Rev.*, 2010, **62**, 1064–1079.
2 D. Peer, J. M. Karp, S. Hong, O. C. FaroKHzad, R. Margalit and R. Langer, *Nat. Nanotechnol.*, 2007, **2**, 751–760.
3 P. S. Yarmolenko, Y. L. Zhao, C. Landon, I. Spasojevic, F. Yuan, D. Needham, B. L. Viglianti and M. W. Dewhirst, *Int. J. Hyperthermia*, 2010, **26**, 485–498.
4 F. S. Farhat, S. Temraz, J. Kattan, K. Ibrahim, N. Bitar, N. Haddad, R. Jalloul, H. A. Hatoum, G. Nsouli and A. I. Shamseddine, *Clin. Breast Cancer*, 2011, **11**, 384–389.
5 N. Casagrande, M. Celegato, C. Borghese, M. Mongiat, A. Colombatti and D. Aldinucci, *Clin. Cancer Res.*, 2014, **20**, 5496–5506.
6 N. Mylonakis, A. Athanasiou, N. Ziras, J. Angel, A. Rapti, S. Lampaki, N. Politis, C. Karanikas and C. Kosmas, *Lung Cancer*, 2010, **68**, 240–247.
7 G. P. Stathopoulos and T. Boulikas, *J. Drug Delivery*, 2012, **2012**, 581363.
8 M. Seleci, D. A. Seleci, T. Scheper and F. Stahl, *Int. J. Mol. Sci.*, 2017, **18**, 1415–1425.

9 Y. N. Dai, J. Z. Su, K. Wu, W. K. Ma, B. Wang, M. X. Li, P. F. Sung, Q. M. Shen, Q. Wang and Q. L. Fan, *ACS Appl. Mater. Interfaces*, 2019, **11**, 10540–10553.
10 K. C. Liu, A. Arivajiagane, S. J. Wu, S. C. Tzou, C. Y. Chen and Y. M. Wang, *Nanomed. Nanotechnol. Biol. Med.*, 2019, **15**, 285–294.
11 H. L. Liu, A. Jablonska, Y. G. Li, S. Y. Cao, D. X. Liu, H. W. Chen, P. C. M. Van Zijl, J. W. M. Bulte, M. Janowski, P. Walczak and G. S. Liu, *Theranostics*, 2016, **6**, 1588–1600.
12 T. Tagami, W. D. Foltz, M. J. Ernsting, C. M. Lee, I. F. Tannock, J. P. May and S. D. Li, *Biomaterials*, 2011, **32**, 6570–6578.
13 G. Mikhaylov, U. Mikac, A. A. Magaeva, V. I. Itin, E. P. Naiden, I. Psakhye, L. Babes, T. Reinheckel, C. Peters, R. Zeiser, M. Bogyo, V. Turk, S. G. Psakhye, B. Turk and O. Vasiljeva, *Nat. Nanotechnol.*, 2011, **6**, 594–602.
14 H. Xu, T. Y. Ohulchanskyy, A. Yakovliev, R. Zinyuk, J. Song, L. W. Liu, J. L. Qu and Z. Yuan, *Theranostics*, 2019, **9**, 1323–1335.
15 N. Beztsinna, Y. Tsvetkova, J. Jose, B. Rhourri-Frih, W. Al Rawashdeh, T. Lammers, F. Kiessling and I. Bestel, *Int. J. Nanomed.*, 2017, **12**, 3813–3825.
16 F. F. Zhao, J. Zhou, X. J. Su, Y. H. Wang, X. S. Yan, S. N. Jia and B. Du, *Small*, 2017, **13**, 1603990.
17 Y. J. Liu and N. Zhang, *Biomaterials*, 2012, **33**, 5363–5375.
18 H. Y. Guo, W. S. Chen, X. Y. Sun, Y. N. Liu, J. Li and J. X. Wang, *Carbohydr. Polym.*, 2015, **118**, 209–217.
19 M. Marciello, J. Pellico, I. Fernandez-Barahona, F. Herranz, J. Ruiz-Cabello and M. Filice, *Interface Focus*, 2016, **6**, 20160055.
20 M. H. Lee, E. J. Kim, H. Lee, H. M. Kim, M. J. Chang, S. Y. Park, K. S. Hong, J. S. Kim and J. L. Sessler, *J. Am. Chem. Soc.*, 2016, **138**, 16380–16387.
21 L. L. Ren, S. Z. Chen, H. D. Li, Z. Y. Zhang, J. P. Zhong, M. L. Liu and X. Zhou, *Acta Biomater.*, 2016, **35**, 260–268.
22 B. S. Ji, M. L. Wang, D. W. Gao, S. S. Xing, L. Li, L. X. Liu, M. Zhao, X. M. Qi and K. Dai, *Nanomedicine*, 2017, **12**, 237–253.
23 S. Mastrogiacomo, A. E. Kownacka, W. Q. Dou, B. P. Burke, R. T. M. de Rosales, A. Heerschap, J. A. Jansen, S. J. Archibald and X. F. Walboomers, *Adv. Healthcare Mater.*, 2018, **7**, 1800202.
24 Y. Kuang, Y. Cao, M. Liu, G. Y. Zu, Y. J. Zhang, Y. Zhang and R. J. Pei, *ACS Appl. Mater. Interfaces*, 2018, **10**, 26099–26107.
25 F. H. Wang, K. Bae, Z. W. Huang and J. M. Xue, *Nanoscale*, 2018, **10**, 5642–5649.
26 A. Banerjee, G. E. Bertolesi, C. C. Ling, B. Blasiak, A. Purchase, O. Calderon, B. Tomanek and S. Trudel, *ACS Appl. Mater. Interfaces*, 2019, **11**, 13069–13078.
27 J. J. Li, C. Wu, P. F. Hou, M. Zhang and K. Xu, *Biosens. Bioelectron.*, 2018, **102**, 1–8.
28 M. M. Wu, Y. M. Xue, N. Li, H. Y. Zhao, B. Lei, M. Wang, J. W. Wang, M. Luo, C. Zhang, Y. P. Du and C. H. Yan, *Angew. Chem., Int. Ed.*, 2019, **58**, 6880–6885.
29 Y. Wang, T. Yang, H. T. Ke, A. J. Zhu, Y. Y. Wang, J. X. Wang, J. K. Shen, G. Liu, C. Y. Chen, Y. L. Zhao and H. B. Chen, *Adv. Mater.*, 2015, **27**, 3874.
30 L. J. Zhou, T. Yang, J. X. Wang, Q. L. Wang, X. Y. Lv, H. T. Ke, Z. Q. Guo, J. K. Shen, Y. Wang, C. G. Xing and H. B. Chen, *Theranostics*, 2017, **7**, 764–774.
31 L. Han, J. M. Xia, X. Hai, Y. Shu, X. W. Chen and J. H. Wang, *ACS Appl. Mater. Interfaces*, 2017, **9**, 6941–6949.
32 K. C. Briley-Saebo, T. H. Nguyen, A. M. Saeboe, Y.-S. Cho, S. K. Ryu, E. Volkava, S. Dickson, G. Leibundgut, P. Weisner, S. Green, F. Casanada, Y. I. Miller, W. Shaw, J. L. Witztum, Z. A. Fayad and S. Tsimikas, *J. Am. Coll. Cardiol.*, 2012, **59**, 1043.
33 H. B. Ruttala and Y. T. Ko, *Pharm. Res.*, 2015, **32**, 1002–1016.
34 E. K. Rowinsky, L. A. Cazenave and R. C. Donehower, *J. Natl. Cancer Inst.*, 1990, **82**, 1247–1259.
35 A. K. Singla, A. Garg and D. Aggarwal, *Int. J. Pharm.*, 2002, **235**, 179–192.
36 M. J. Gu, K. F. Li, L. X. Zhang, H. Wang, L. S. Liu, Z. Z. Zheng, N. Y. Han, Z. J. Yang and T. Y. Fan, *Int. J. Nanomed.*, 2015, **10**, 5187–5204.
37 Y. Dai, A. P. Zhang, J. You, J. J. Li, H. T. Xu and K. Xu, *RSC Adv.*, 2015, **5**, 77204–77210.
38 T. Yang, F. D. Cui, M. K. Choi, J. W. Cho, S. J. Chung, C. K. Shim and D. D. Kim, *Int. J. Pharm.*, 2007, **338**, 317–326.
39 G. Moku, S. K. Gulla, N. V. Nimmu, S. Khalid and A. Chaudhuri, *Biomater. Sci.*, 2016, **4**, 627–638.
40 A. D. Bangham, J. De Gier and G. D. Greville, *Chem. Phys. Lipids*, 1967, **1**, 225–246.
41 H. P. Luehmann, E. D. Pressly, L. Detering, C. Wang, R. Pierce, P. K. Woodard, R. J. Gropler, C. J. Hawker and Y. J. Liu, *J. Nucl. Med.*, 2014, **55**, 629–634.
42 E. Nogueira, A. C. Gomes, A. Preto and A. Cavaco-Paulo, *Colloids Surf., B*, 2015, **136**, 514–526.
43 Y. W. Jun, Y. M. Huh, J. S. Choi, J. H. Lee, H. T. Song, S. Kim, S. Yoon, K. S. Kim, J. S. Shin, J. S. Suh and J. Cheon, *J. Am. Chem. Soc.*, 2005, **127**, 5732–5733.
44 J. A. Peters, J. Huskens and D. J. Raber, *Prog. Nucl. Magn. Reson. Spectrosc.*, 1996, **28**, 283–350.
45 S. H. Koenig and R. D. Brown, *Prog. Nucl. Magn. Reson. Spectrosc.*, 1990, **22**, 487–567.
46 A. Yilmaz, M. Z. Koylu and E. Uysal, *Appl. Magn. Reson.*, 2009, **35**, 601–612.
47 S. Langereis, A. Dirksen, T. M. Hackeng, M. H. P. van Genderen and E. W. Meijer, *New J. Chem.*, 2007, **31**, 1152–1160.
48 D. P. J. Pan, A. H. Schmieder, S. A. Wickline and G. M. Lanza, *Tetrahedron*, 2011, **67**, 8431–8444.
49 T. Kim, E. Momin, J. Choi, K. Yuan, H. Zaidi, J. Kim, M. Park, N. Lee, M. T. McMahon, A. Quinones-Hinojosa, J. W. M. Bulte, T. Hyeon and A. A. Gilad, *J. Am. Chem. Soc.*, 2011, **133**, 2955–2961.
50 C. R. Ireson and L. R. Kelland, *Mol. Cancer Ther.*, 2006, **5**, 2957–2962.
51 M. Ashrafuzzaman, *BioMed Res. Int.*, 2014, 697923.
52 F. F. Li, J. Lu, J. Liu, C. Liang, M. L. Wang, L. Y. Wang, D. F. Li, H. Z. Yao, Q. L. Zhang, J. Wen, Z. K. Zhang, J. Li, Q. X. Lv, X. J. He, B. S. Guo, D. G. Guan, Y. Y. Yu, L. Dang, X. H. Wu, Y. S. Li, G. F. Chen, F. Jiang, S. G. Sun,

B. T. Zhang, A. P. Lu and G. Zhang, *Nat. Commun.*, 2017, **8**, 1390.

53 S. Koudelka and J. Turanek, *J. Controlled Release*, 2012, **163**, 322–334.

54 S. Kaida, H. Cabral, M. Kumagai, A. Kishimura, Y. Terada, M. Sekino, I. Aoki, N. Nishiyama, T. Tani and K. Kataoka, *Cancer Res.*, 2010, **70**, 7031–7041.

55 H. J. Yoon, E. S. Lee, M. Kang, Y. Jeong and J. H. Park, *J. Mater. Chem. B*, 2015, **3**, 2935–2938.

56 D. Chen, B. W. Li, S. H. Cai, P. Wang, S. W. Peng, Y. Z. Sheng, Y. Y. He, Y. Q. Gu and H. Y. Chen, *Biomaterials*, 2016, **100**, 1–16.

57 Y. Y. Wang, X. Chen, B. Q. Tian, J. F. Liu, L. Yang, L. L. Zeng, T. F. Chen, A. Hong and X. G. Wang, *Theranostics*, 2017, **7**, 1360–1372.

58 J. M. Zhang, R. I. E. Chen, X. F. Fang, F. Q. Chen, Y. T. Wang and M. W. Chen, *Nano Res.*, 2015, **8**, 201–218.

59 J. Carvalho, A. Paiva, M. P. C. Campello, A. Paulo, J. L. Mergny, G. F. Salgado, J. A. Queiroz and C. Cruz, *Sci. Rep.*, 2019, **9**, 7945.

60 L. Y. Li, J. J. Hou, X. J. Liu, Y. J. Guo, Y. Wu, L. H. Zhang and Z. J. Yang, *Biomaterials*, 2014, **35**, 3840–3850.

61 H. C. Fischer, L. C. Liu, K. S. Pang and W. C. W. Chan, *Adv. Funct. Mater.*, 2006, **16**, 1299–1305.